Circulation

ORIGINAL RESEARCH ARTICLE

Large Cardiac Muscle Patches Engineered From Human Induced-Pluripotent Stem Cell–Derived Cardiac Cells Improve Recovery From Myocardial Infarction in Swine

BACKGROUND: Here, we generated human cardiac muscle patches (hCMPs) of clinically relevant dimensions (4 cm × 2 cm × 1.25 mm) by suspending cardiomyocytes, smooth muscle cells, and endothelial cells that had been differentiated from human induced-pluripotent stem cells in a fibrin scaffold and then culturing the construct on a dynamic (rocking) platform.

METHODS: In vitro assessments of hCMPs suggest maturation in response to dynamic culture stimulation. In vivo assessments were conducted in a porcine model of myocardial infarction (MI). Animal groups included: MI hearts treated with 2 hCMPs (MI+hCMP, n=13), MI hearts treated with 2 cell-free open fibrin patches (n=14), or MI hearts with neither experimental patch (n=15); a fourth group of animals underwent sham surgery (Sham, n=8). Cardiac function and infarct size were evaluated by MRI, arrhythmia incidence by implanted loop recorders, and the engraftment rate by calculation of quantitative polymerase chain reaction measurements of expression of the human Y chromosome. Additional studies examined the myocardial protein expression profile changes and potential mechanisms of action that related to exosomes from the cell patch.

RESULTS: The hCMPs began to beat synchronously within 1 day of fabrication, and after 7 days of dynamic culture stimulation, in vitro assessments indicated the mechanisms related to the improvements in electronic mechanical coupling, calcium-handling, and force generation, suggesting a maturation process during the dynamic culture. The engraftment rate was 10.9±1.8% at 4 weeks after the transplantation. The hCMP transplantation was associated with significant improvements in left ventricular function, infarct size, myocardial wall stress, myocardial hypertrophy, and reduced apoptosis in the periscar boarder zone myocardium. hCMP transplantation also reversed some MI-associated changes in sarcomeric regulatory protein phosphorylation. The exosomes released from the hCMP appeared to have cytoprotective properties that improved cardiomyocyte survival.

CONCLUSIONS: We have fabricated a clinically relevant size of hCMP with trilineage cardiac cells derived from human induced-pluripotent stem cells. The hCMP matures in vitro during 7 days of dynamic culture. Transplantation of this type of hCMP results in significantly reduced infarct size and improvements in cardiac function that are associated with reduction in left ventricular wall stress. The hCMP treatment is not associated with significant changes in arrhythmogenicity.

Ling Gao, PhD
Zachery R. Gregorich, PhD
Wuqiang Zhu, MD, PhD
Saidulu Mattapally, PhD
Yasin Oduk, PhD
Xi Lou, BS
Ramaswamy Kannappan, PhD
Anton V. Borovjagin, PhD
Gregory P. Walcott, PhD
Andrew E. Pollard, PhD
Vladimir G. Fast, PhD
Xinyang Hu, MD, PhD
Steven G. Lloyd, MD, PhD
Ying Ge, PhD
Jianyi Zhang, MD, PhD

Key Words: heart ■ models, animal ■ myocardial infarction ■ pluripotent stem cells ■ tissue engineering

Sources of Funding, see page 1729

http://circ.ahajournals.org

Clinical Perspective

What Is New?

- Human cardiac muscle patches (hCMPs) of clinically relevant dimensions (4 cm × 2 cm × 1.25 mm) were generated by suspending cardiomyocytes, smooth muscle cells, and endothelial cells that had been differentiated from human induced-pluripotent stem cells in a fibrin matrix and culturing the construct on a dynamic (rocking) platform.
- The results from in vitro assessments of calcium transients, action potential propagation, and force generation, and the presence of intercalated disk-like structures, as well, suggest that cardiomyocytes mature in the hCMP during the 7-day dynamic culture period.

What Are the Clinical Implications?

- We present hCMPs with larger dimensions.
- After fabrication and culture on a dynamic, rocking platform, the electrophysiological and contractile properties of the hCMPs resembled those of native myocardial tissue.
- When 2 of the hCMPs were transplanted onto infarcted swine heart, measurements of cardiac function, infarct size, and wall stress improved significantly with no increase in the occurrence of arrhythmogenic complications. Changes in the expression profile of myocardial proteins indicated that hCMP transplantation partially reversed abnormalities in sarcomeric protein phosphorylation.
- Collectively, these observations indicate that hCMPs of clinically relevant dimensions can be successfully generated and may improve recovery from ischemic myocardial injury.

The human induced-pluripotent stem cell (hiPSC) technology has advanced medical science significantly. A number of studies have shown that when hiPSCs are differentiated into cardiomyocytes and evaluated in rodent, swine, and nonhuman primate models of myocardial infarction (MI), the treatment is associated with functional improvement.[1–4] However, in nonhuman primate models of MI, when the dose and grafts are large enough, the cardiomyocytes derived from human embryonic stem cells or nonhuman primate iPSCs have been associated with increased incidences of ventricular arrhythmias.[2,5] The hiPSCs and human embryonic stem cells are pluripotent stem cells (PSCs), and PSC-derived cardiomyocytes are structurally and functionally similar to neonatal cardiomyocytes,[6,7] which may limit their contractile activity and could lead to electric instability after graft into recipient adult hearts. The previously reported preclinical trials of cardiac tissue–engineering therapy of rodent models used relatively small and thin fabricated cardiovascular tissues,[8] which are limitations from the clinical perspective. Thus, methods for fabrication of larger and thicker functional cardiac tissue, and methods for promoting the maturation of cardiomyocytes derived from hPSCs are urgently needed.

Cardiac tissue patch–based approaches for cell delivery are more effective from the engraftment rate perspective because of the unique characteristics of the high pressure and high flow of the left ventricle (LV).[8–13] Cardiac muscle patch could also provide the structure strengthening the injured LV, thereby preventing the LV dilation and the overstretching of the border zone (BZ) myocardium.[1,6,12,14,15] It is noteworthy that the cardiomyocytes present in 3-dimensional, engineered human cardiac muscle patches (hCMPs) are more mature than those obtained via monolayer-culturing techniques,[6,11,16] and hiPSC-derived cardiomyocytes (hiPSC-CMs) assumed a more mature and structurally aligned phenotype after transplantation when the hiPSCs were reprogrammed from cardiac-lineage cells (hciPSCs) rather than from dermal fibroblasts or umbilical cord blood mononuclear cells.[17] However, most of the hiPSC-hCMPs have been too small and too thin from the translational perspective.[1,18,19]

Previously, we have shown that cardiomyocytes (CMs) are more resistant to hypoxic injury when cocultured with endothelial cells (ECs) and smooth muscle cells (SMCs) than when cultured alone,[3,20] and that the engraftment of transplanted CMs, and measurements of myocardial perfusion, metabolism, and contractile activity, as well, improves when the cells are coadministered with ECs and SMCs.[3] Thus, for the experiments described in this report, hiPSC-derived CMs, ECs (hiPSC-ECs), and SMCs (hiPSC-SMCs) were differentiated from hciPSCs,[17] seeded into a 3-dimensional fibrin scaffold to fabricate a novel type of hCMP with clinically relevant size and thickness (4 cm × 2 cm × 1.25 mm), and subsequently cultured with dynamic and mechanical stimulation to promote maturation. The effectiveness of these hCMPs for improving cardiac function after myocardial injury was then evaluated in a large-animal model of MI.

METHODS

The data, analytic methods, and study materials are made available to other researchers for purposes of reproducing the results or replicating the procedure. (See Gao Ling. Large Cardiac-muscle Patches [Internet]. 2017. https://osf.io/hrzjb/). A detailed description of the experimental procedures used in this study is provided in the online-only Data Supplement. All procedures and protocols involving animals were approved by the Institutional Animal Care and Use Committee of the University of Alabama at Birmingham and performed in accordance with the National Research Council's Guide for the Care and Use of Laboratory Animals.

Statistical Analysis

All values are expressed as mean±SEM, and were tested for significance level of type I error ($P<0.05$) via the Student t test

or ANOVA for differences between the values. The Bonferroni correction for the significance level was used to take into account of multiple comparisons.

RESULTS

Differentiation and Characterization of hiPSC-CMs, -SMCs, and -ECs

hiPSCs were reprogrammed from human cardiac fibroblasts, engineered to express green fluorescent protein (GFP) (Figure 1A through 1C), and then differentiated into hiPSC-CMs, -ECs, and -SMCs as previously reported.[3,21–23] Spontaneous contractions (Movie I in the online-only Data Supplement) were typically observed in hiPSC-CMs on day 8 after differentiation was initiated, and the number of contracting cells usually increased up to day 12. One week after purification, the hiPSC-CMs (Figure 1D through 1I) expressed cardiac troponin T (cTnT), α sarcomeric actinin (αActinin), α-sarcomeric actin, slow cardiac myosin heavy chain, cardiac troponin I (cTnI), and ventricular myosin light chain 2; the gap-junction protein cardiac connexin 43 (Con43) was commonly observed between adjacent cells. hiPSC-SMCs (Figure 1J through 1L) and hiPSC-ECs (Figure 1M through 1O) expressed SMC-specific (α smooth muscle actin [αSMA], calponin 1, and smooth muscle 22 alpha) and EC-specific (CD31, vascular endothelial cadherin, and von Willebrand factor) markers, respectively, and when stimulated with vascular endothelial growth factor, the hiPSC-ECs formed tube-like structures in Matrigel (Figure IA in the online-only Data Supplement). Flow cytometry analysis confirmed that each of the final hiPSC-derived cell populations was at least 90% pure: 96.4% of the hiPSC-CMs expressed cTnT (Figure IB in the online-only Data Supplement), 91.5% of the hiPSC-SMCs expressed αSMA (Figure IC in the online-only Data Supplement), and >95% of the hiPSC-ECs expressed CD31 and vascular endothelial cadherin (Figure ID and IE in the online-only Data Supplement).

Fabrication and Characterization of Large, Thick, hiPSC-Derived hCMPs

Large, thick hCMPs (4 cm × 2 cm × 1.25 mm) were fabricated in vitro by mixing a fibrinogen solution containing 4 million hiPSC-CMs, 2 million hiPSC-ECs, and 2 million hiPSC-SMCs with thrombin, and then quickly adding the mixture to a mold (Figure 2A).The mixture solidified within a few minutes, and the patches were cultured on a dynamic (rocking, 45 rpm) platform for 7 days before subsequent in vitro analyses were performed (Movie II in the online-only Data Supplement).The hiPSC-CMs began to beat synchronously across the entire hCMP within 1 day of seeding (Movie III in the online-only Data Supplement); by day 7, the amplitude of contraction was noticeably greater (Movie IV in the online-only Data Supplement), whereas the expression of genes required for contractile function (cTnT, cTnI, α-myosin heavy chain, and cardiac actin 1) and for generating calcium transients (ryanodine receptor 2, sarcoplasmic/endoplasmic reticulum calcium ATPase 2, Con43) was significantly greater in the hCMPs than in monolayers of equivalent populations of hiPSC-derived cardiac cells (Figure II in the online-only Data Supplement, Table I in the online-only Data Supplement). cTnT, cTnI, ryanodine receptor 2, and sarcoplasmic/endoplasmic reticulum calcium ATPase 2 protein levels were also greater in the dynamically cultured hCMPs than in hCMPs that had been grown under static culture conditions (Figure IIIA and IIIB in the online-only Data Supplement), and observations of hCMPs stained with phalloidin (Figure 2B) (to visualize F-actin) or hematoxylin and eosin (Figure 2C) suggested that they could be easily permeated by the culture medium. Less than 5% of the cells displayed evidence of apoptosis or necrosis (ie, positive staining for terminal deoxynucleotidyltransferase dUTP nick end labeling or phosphorylated mixed lineage kinase domain like pseudokinase, respectively) (Figure 2D and 2E), whereas analysis of hCMPs that had been stained for the endothelial marker CD31, the SMC marker αSMA, and the CM-specific protein cTnI confirmed that the 3 cell types interacted with each other (Figure 2F, Figure IIIC in the online-only Data Supplement), and that the original 2:1:1 ratio of hiPSC-CMs, -SMCs, and -ECs was largely retained at day 7 (Figure 2G). Con43 expression was prevalent throughout the hCMPs (Figure 2H), suggesting that the hiPSC-CMs were strongly interconnected, and structures that resembled primitive intercalated discs with stress-transmitting fascia adherens junctions and desmosomes were visible in transmission electron microscopy (Figure 2I).

Functional Assessment of hCMPs In Vitro

Optical mapping studies confirmed that the transmembrane potential of the hCMPs could be paced at cycle lengths ranging from 1000 ms to 450 ms (Figure 3A). When paced at 800 ms (Figure 3B and 3C), the average conduction velocity was 14.1±1.0 cm/s; the average durations of the action potential until 50% and 80% repolarization were 179±15 and 231±15 ms, respectively; and the average Ca^{2+} transient durations until 50% and 80% relaxation were 189±15 and 276±23 ms, respectively (Figure 3D). Furthermore, when a linear array system of electric sensors was used to evaluate intercellular coupling (Figure 3E), the results from assessments in the hCMPs were similar to those in myocardium from the left ventricles of rabbits (Figure 3F). The data suggest that gap-junction communication in the hCMPs at day 7 of dynamic culture is comparable to that observed in native myocardium, at least from the perspective of intercellular impedance.

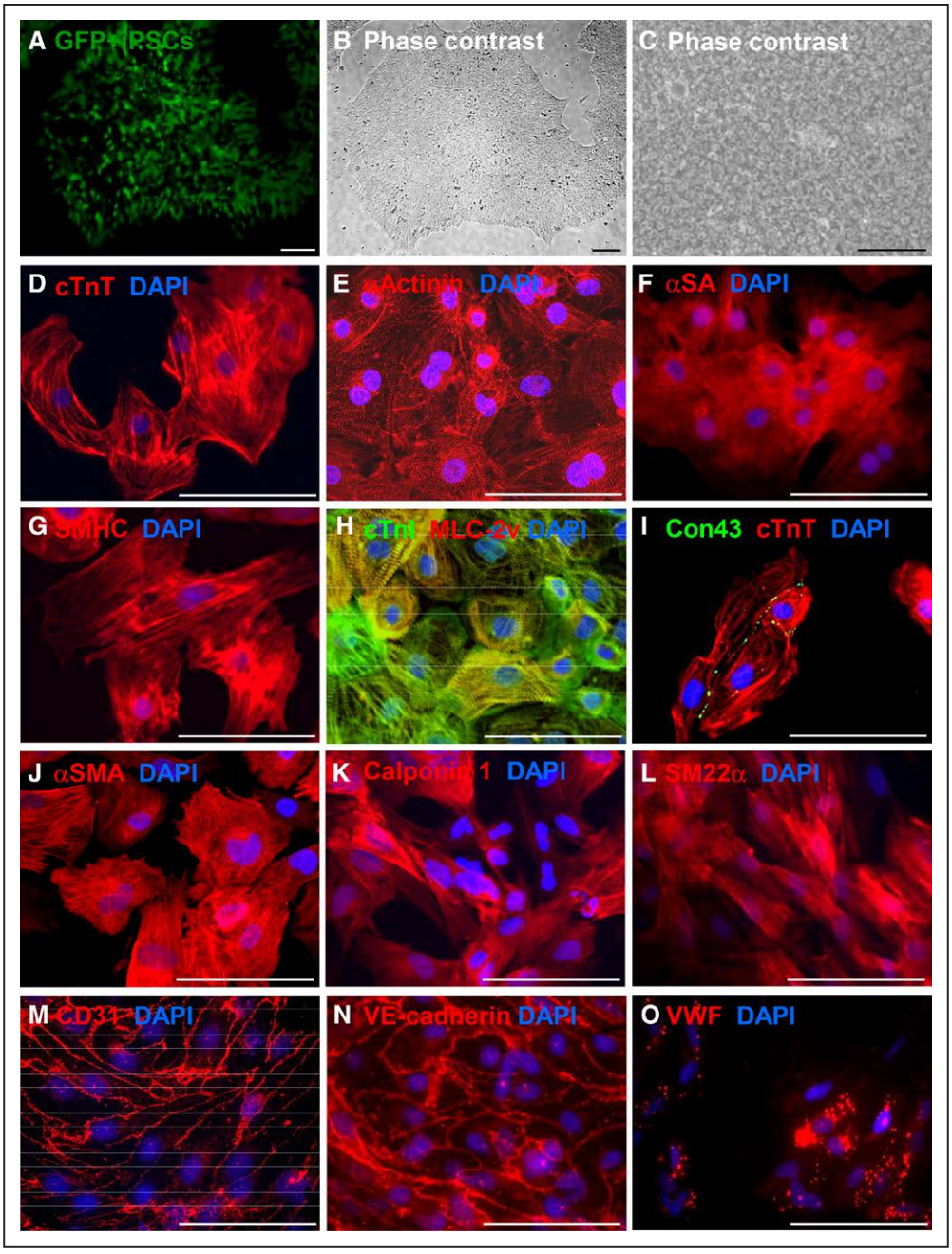

Figure 1. Characterization of human induced-pluripotent stem cells (hiPSCs) and hiPSC-derived cardiac cells. **A**, The hiPSCs used for this investigation were reprogrammed from human left atrial fibroblasts and engineered to express green fluorescent protein (GFP). When cultured as a monolayer with Matrigel, the cells grew to form flat, compact colonies with distinct cell borders (magnification: 40×) (**B**) and displayed the morphological characteristics of hiPSCs, including prominent nuclei and a high nucleus-to-cytoplasm ratio (magnification: 100×) (**C**). **D** through **I**, hiPSC-derived cardiomyocytes (hiPSC-CMs) were characterized via immunofluorescent analyses of cardiac troponin T (cTnT) (**D**), α-sarcomeric actinin (αActinin) (**E**), α-sarcomeric actin (αSA) (**F**), slow myosin heavy chain (SMHC) (**G**), cardiac troponin I (cTnI) and myosin light chain 2v (MLC-2v) (**H**), and connexin43 (Con43) and cTnT expression (**I**). **J** through **L**, hiPSC-derived smooth muscle cells (hiPSC-SMCs) were characterized via immunofluorescent analyses of α-smooth muscle actin (αSMA) (**J**), calponin 1(**K**), and smooth muscle 22 alpha (SM22α) expression (**L**). **M** through **O**, hiPSC-derived endothelial cells (hiPSC-ECs) were characterized via immunofluorescent analyses of CD31 (**M**), vascular endothelial cadherin (VE-cadherin) (**N**), and von Willebrand factor (VWF) (**O**) expressions. Nuclei were counterstained with 4′,6-diamidino-2-phenylindole (DAPI). Bar=100 μm.

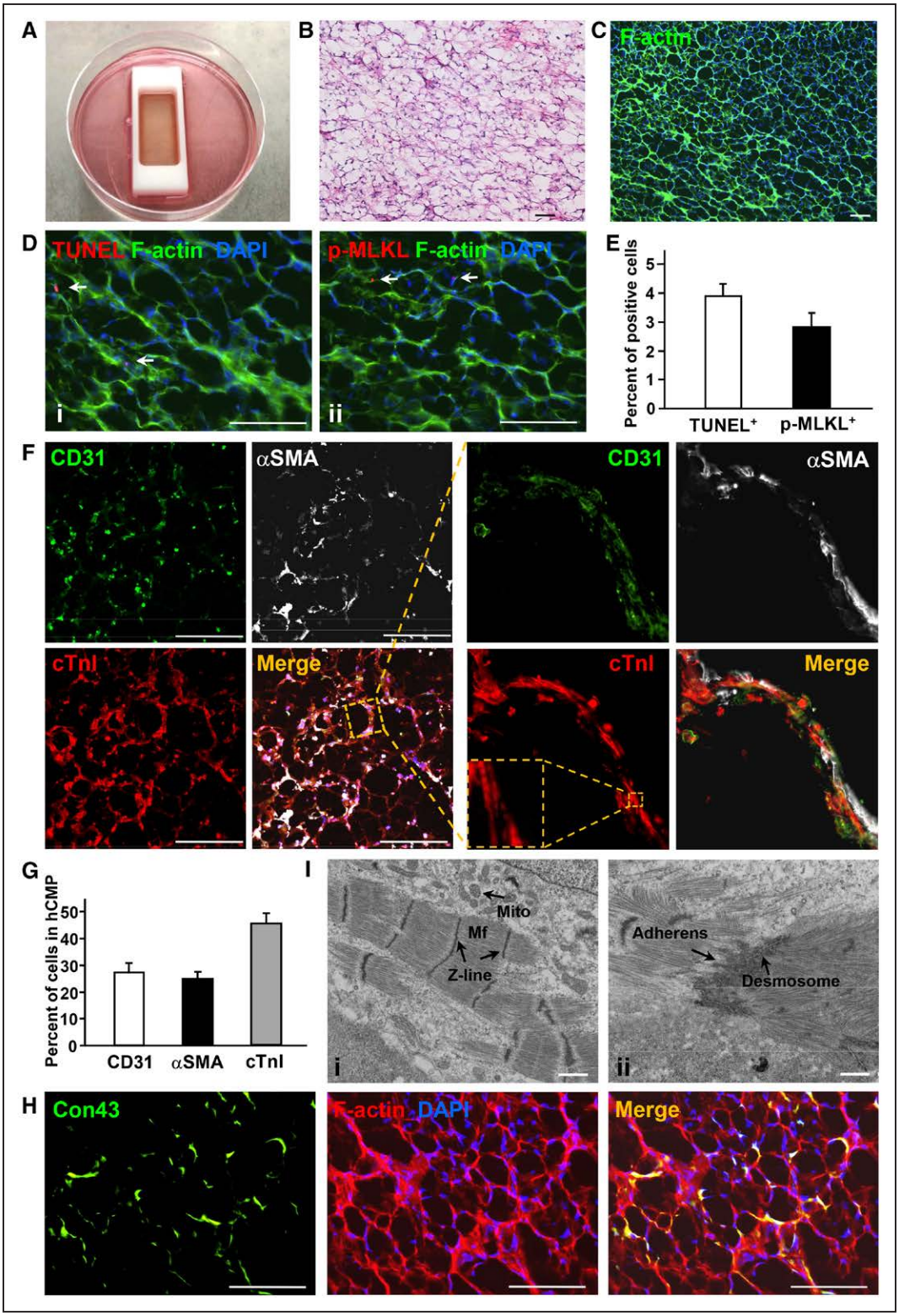

Figure 2. Characterization of the structure and cellular composition of the human cardiac muscle patch (hCMP). **A**, Large hCMPs (4 cm × 2 cm × 1.25 mm) were fabricated by suspending 4 million hiPSC-CMs, 2 million hiPSC-ECs, and 2 million hiPSC-SMCs in a fibrinogen solution, mixing the cell-containing fibrinogen solution with a thrombin solution, quickly pouring the mixture into a mold (internal dimensions: 4 cm×2 cm×1 cm), and then culturing the cells for 1 week. **B** and **C**, The internal structure of the hCMP was evaluated via hematoxylin/eosin staining (**B**) and phalloidin staining (**C**) to identify the presence of F-actin (bar= 00 μm). **D**, Apoptotic and necrotic cells were identified via terminal deoxynucleotidyl transferase dUTP nick end labeling (TUNEL) (**Di**) and immunofluorescence staining (**Dii**) for a phosphorylated mixed lineage kinase (*Continued*)

The functional maturation of the hCMPs was evaluated via measurements of force generation. Spontaneous twitch-force generation (Figure 3G) was weak at slack length (ie, in the absence of stretching), but increased in magnitude as the hCMPs were stretched in 3% increments to 121% of its original slack length (Figure 3H). This finding is consistent with observations that the force of ventricular contraction increases as the muscle fibers stretch in response to larger amounts of blood entering the ventricle (ie, the Frank-Starling mechanism).[24] Spontaneous twitch-force transients (at 110% of slack length) also disappeared on incubation with a reversible inhibitor of the actin-myosin interaction (30 mmol/L 2,3-butanedione monoxime) but reappeared after the inhibitor was washed out of the medium (Figure IV in the online-only Data Supplement), suggesting that hCMP has a normal function in response to cross-bridge inhibition. Studies of pacing-induced contractions indicated that as the frequency increased from 1 to 3 Hz, the magnitude of force generation declined slightly, but not significantly, in the hCMPs (Figure 3I and 3J), which reflects a superior contractile functional benefits of this hCMP with trilineage cardiac cells from hciPSCs,[17] with the best ever positive force-frequency relationship than previous hiPSC-hCMP, and similar to what have been observed in adult human CMs.[1,6,10] This may be because of maturation of the sarcoplasmic reticulum in the dynamic culture system. Furthermore, force generation in the hCMPs increased in response to higher extracellular calcium concentrations (Figure V in the online-only Data Supplement) and when the hCMPs were cultured with a β-adrenergic agonist (isoproterenol) (Figure 3K and 3L). Collectively, these observations suggest that the force-generation and calcium-handling machinery of the hCMPs was relatively further developed within hCMP in the dynamic culture. It is noteworthy that the total amount of force generated by the hCMPs did not differ significantly from the force generated by patches that contained the same total number of cells but were composed of only hiPSC-CMs (Figure 3M); thus, the amount of force generated per CM was approximately twice as great in the hCMPs (Figure 3N). Collectively, these observations indicate that the hCMPs were electrically integrated and exhibited significant functional maturation after 7 days of dynamic culture.

hiPSC-Derived Cardiac Cells Engraft and Survive After hCMP Transplantation Into a Porcine Model of MI

The cardioprotective efficiency of hCMP transplantation was evaluated in a porcine model of MI. MI was surgically induced by occluding the distal left anterior descending coronary artery for 60 minutes before reperfusion, and then 2 hCMPs were sutured over the site of infarction in animals from the MI+hCMP group (Movie V in the online-only Data Supplement). Two large cell-free open fibrin patches (OPs), which were otherwise identical to the hCMPs, were sutured over the injury site in animals from the MI+OP group, whereas animals in the MI group recovered without either experimental treatment. A fourth group of animals, the Sham group, underwent all surgical procedures for MI induction, with the exception of coronary occlusion (Table II in the online-only Data Supplement). Because the experiments were performed with female pigs, while the transplanted cells were generated from the tissues of male humans and engineered to express GFP, the engraftment and survival rates of the transplanted cells were evaluated via quantitative polymerase chain reaction assessments for the human Y chromosome, and the lineages of the surviving cells were determined via immunofluorescent analyses of the expression of GFP, cTnI, αSMA, cTnT, CD31, human nuclear antigen, αActinin, and the human-specific isoforms of cTnT (hcTnT), calponin 1 (hCalponin 1), and CD31 (hCD31) (Figure 4). The engraftment rate was ≈11% (10.9±1.8%, n=6 hearts) at week 4 after treatment, and all 3 transplanted cell lineages were present in the treated region. Furthermore, GFP^+ cells were generally found in clusters (Figure 4A) and interspersed with αSMA^+ (Figure 4B) and $CD31^+$ (Figure 4C) structures, indicating that the hCMPs were vascularized (Figure 4D), whereas the hiPSC-CMs (Figure 4E), although structurally immature, displayed some evidence of sarcomeric organization (Figure 4F). However, only a small proportion (≈10%) of the vessels in the patch expressed GFP (Figure 4G), hCalponin 1 (Figure 4H), or hCD31 (Figures 4I and 4J). These data demonstrate that the hiPSC-ECs and -SMCs do incorporate, to a small extent, to the vasculature as the native vessels sprouting into the grafted hCMPs, which is consistent with our previous observations in rodent studies.[25,26]

Figure 2 Continued. domain like pseudokinase (p-MLKL), respectively (bar=100 μm), and then quantified as the percentage of cells that were positive for each stain (n=4 hCMPs) (**E**). **F**, ECs, SMCs, and CMs were identified in the hCMP via immunofluorescence staining for the presence of CD31, αSMA, and cTnI, respectively (bar=300 μm); then, the percentage of cells that stained positively for each marker was calculated (n=4 hCMPs) (**G**). **H**, Gap-junctions between adjacent cardiac cells were identified in hCMPs stained for the presence of F-actin and Con43 (bar= 00 μm). **I**, The ultrastructure of the hCMP was analyzed by transmission electron microscope to identify myofibrils (Mf), Z-lines, and mitochondria (Mito) (**Ii**) and primitive intercalated disc-like structures with fascia adherens junctions and desmosomes (**Iii**). Scale bar=1 μm. Con43 indicates connexin43; cTnI, cardiac troponin I; DAPI, 4′,6-diamidino-2-phenylindole; hiPSC, human induced-pluripotent stem cell; hiPSC-CMs, hiPSC-derived cardiomyocytes; hi-PSC-EC, hiPSC-derived endothelial cell; hi-PSC-SMC, hiPSC-derived smooth muscle cell; and αSMA, α-smooth muscle actin.

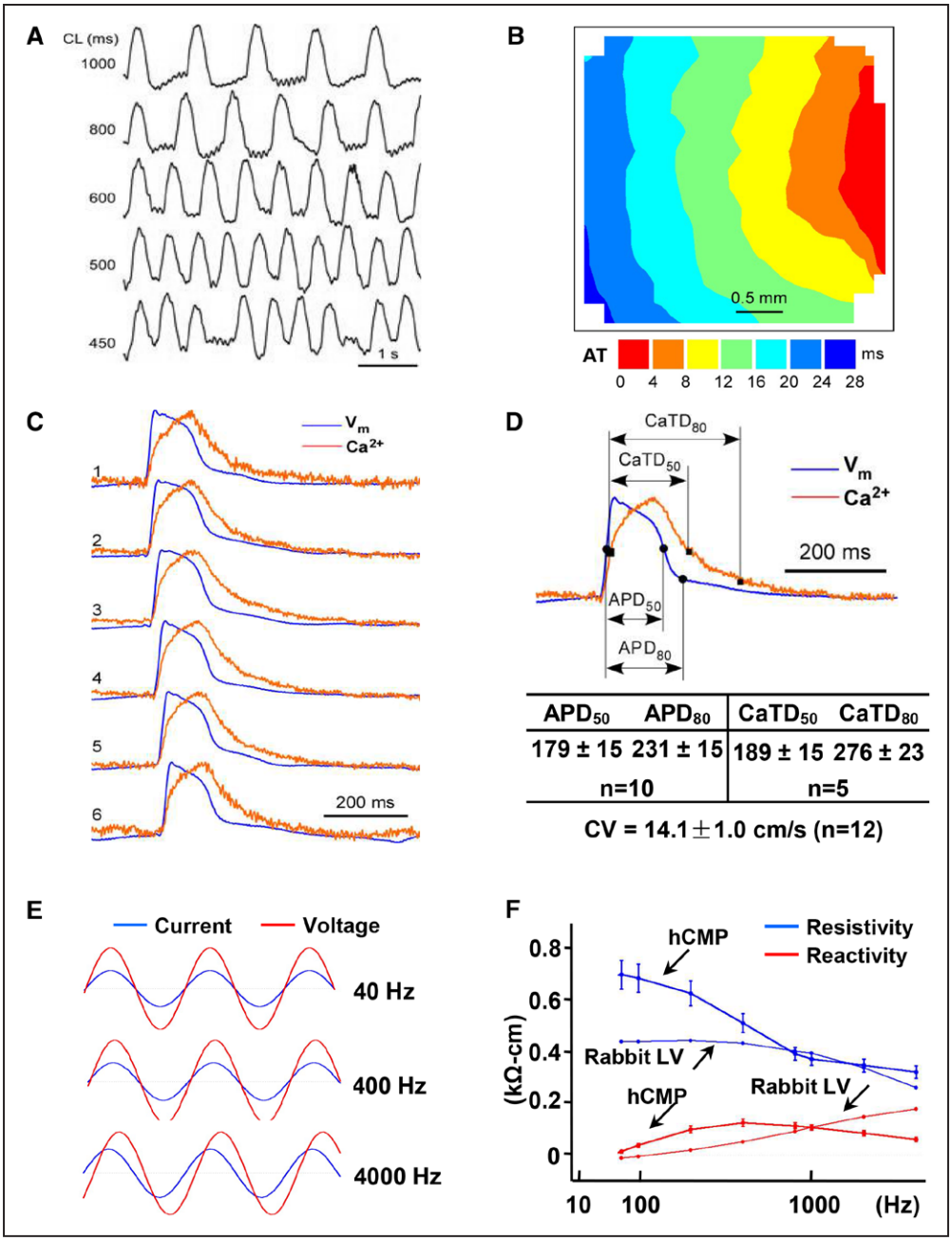

Figure 3. Characterization of hCMP electrophysiology and function.

A through **D**, Action potential (AP) propagation and Ca^{2+} transient kinetics were evaluated in hCMPs 7 days after manufacture by staining hCMPs with a voltage-sensitive dye (RH-237, for AP assessments) or a Ca^{2+}-sensitive dye (Cal-520FF, for Ca^{2+} transient measurements) and then measuring the intensity of transmitted light. **A**, Traces (ie, light intensity) were recorded at the indicated cycle lengths (CLs). Isochronal maps of AP propagation (AT: activation time) (**B**) and optical traces of membrane potential (V_m, blue) and Ca^{2+} transient traces (red) (**C**) were recorded during pacing at CL=800 ms and used to determine the conduction velocity (CV), duration of the action potential until 50% and 80% repolarization (APD_{50} and APD_{80}, respectively), and the duration of the Ca^{2+} transients until 50% and 80% relaxation ($CaTD_{50}$ and $CaTD_{80}$, respectively) (**D**). **E**, Voltage (red) and current (blue) recordings were obtained in hCMPs during stimulation at 40 Hz, 400 Hz, and 4000 Hz; recordings were windowed to enable the current and voltage traces to be compared across 1.5 cycles for each frequency. **F**, Tissue resistivity and reactivity in the hCMPs and in rabbit ventricular myocardium (from a previous report[39]) were summarized as a function of stimulation frequency. **G** through **L**, hCMP force-generation measurements were determined 7 days after hCMP generation. **G**, The relationship between force generation and tensile strain was evaluated by recording force traces as the hCMP was stretched from 100% to 121% of slack length over a 4-minute period. **H**, Active and passive force generation was summarized as a function of hCMP length. **I**, hCMPs were stretched to 110% of slack length, and force traces were recorded as the hCMPs beat spontaneously (s) or in response to electronic pacing at frequencies of 1, 2, and 3 Hz. **J**, Twitch force (*Continued*)

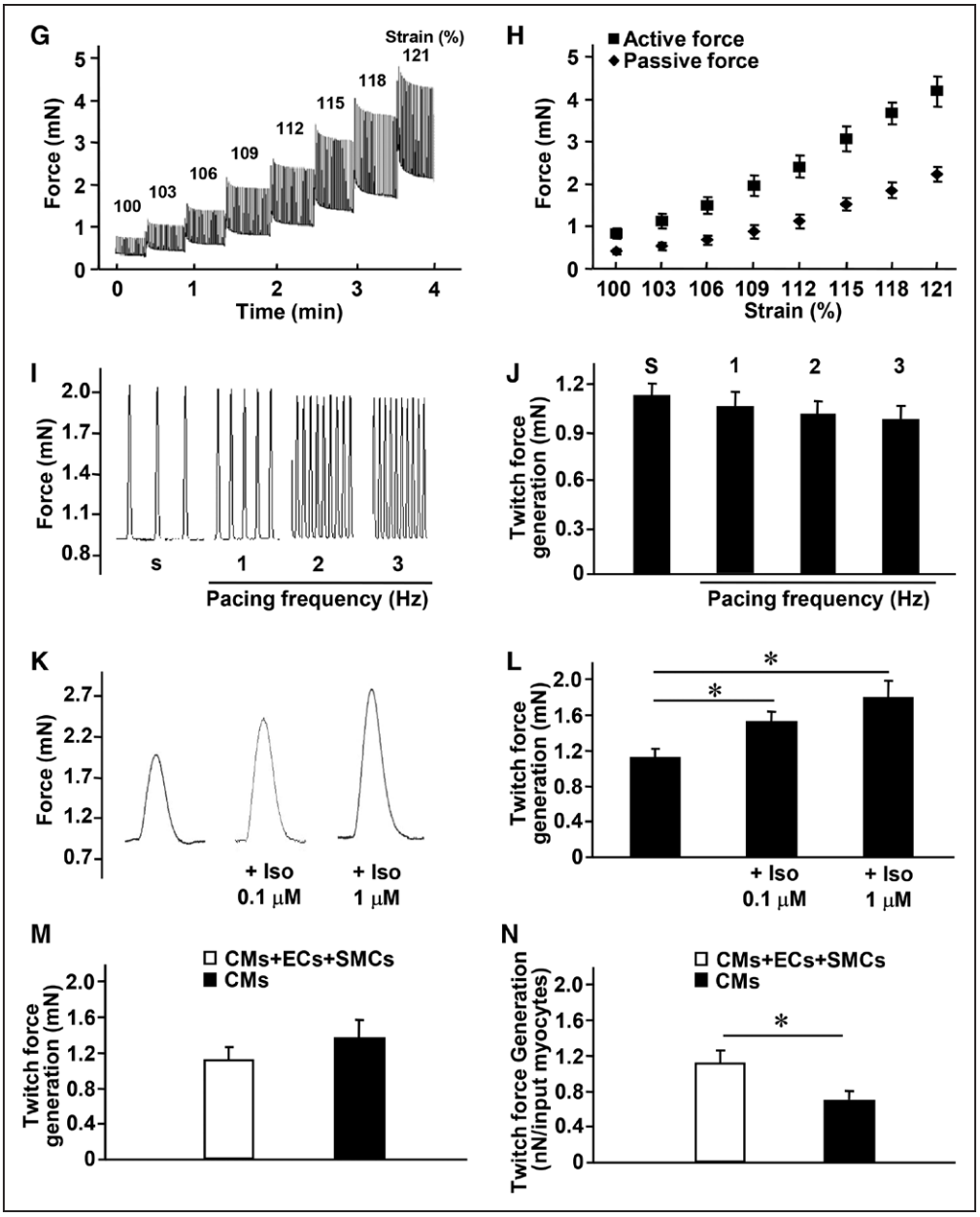

Figure 3 Continued. was summarized as a function of pacing frequency. **K**, hCMPs were stretched to 110% of slack length, and force traces were recorded as the hCMPs beat in the presence of increasing concentrations (0, 0.1 μmol/L, 1 μmol/L) of isoproterenol. **L**, Twitch force was summarized as a function of isoproterenol concentration. **M** and **N**, Twitch force was measured at 110% of slack length in hCMPs and in patches that lacked hiPSC-SMCs and -ECs but were otherwise identical to the hCMPs; then, force generation was calculated for the entire hCMP or patch (**M**) and per cardiomyocyte in the hCMP or the patch (N). **P*<0.05. n=4 to 5 in each group. CM indicates cardiomyocyte; EC, endothelial cell; hCMP, human cardiac muscle patch; ISO, isoproterenol; LV, left ventricle; and SMC, smooth muscle cell.

hCMP Transplantation Improves Myocardial Performance, Regional Wall Stress, and Limits Adverse Remodeling After MI

Cardiac function was evaluated 4 weeks after injury via MRI (Figure 5A) and hemodynamic analysis. Measurements of left ventricular (LV) end-diastolic volume (Figure 5B), LV ejection fraction (Figure 5C), infarct size (Figure 5D), systolic thickening fractions in the infarcted zone of the LV wall and in the periscar border zone (BZ) of the infarct (Figure 5E), LV systolic pressure (Figure 5F), and regional wall stress in both the infarcted zone and BZ (Figure 5G) were significantly better in MI+hCMP animals than in animals from either the MI+OP or MI group. Furthermore, the ratio of LV weight to body-weight (Figure 5H), and the cross-sectional area of CMs located in the BZ (Figure 5I and 5J), as well, in

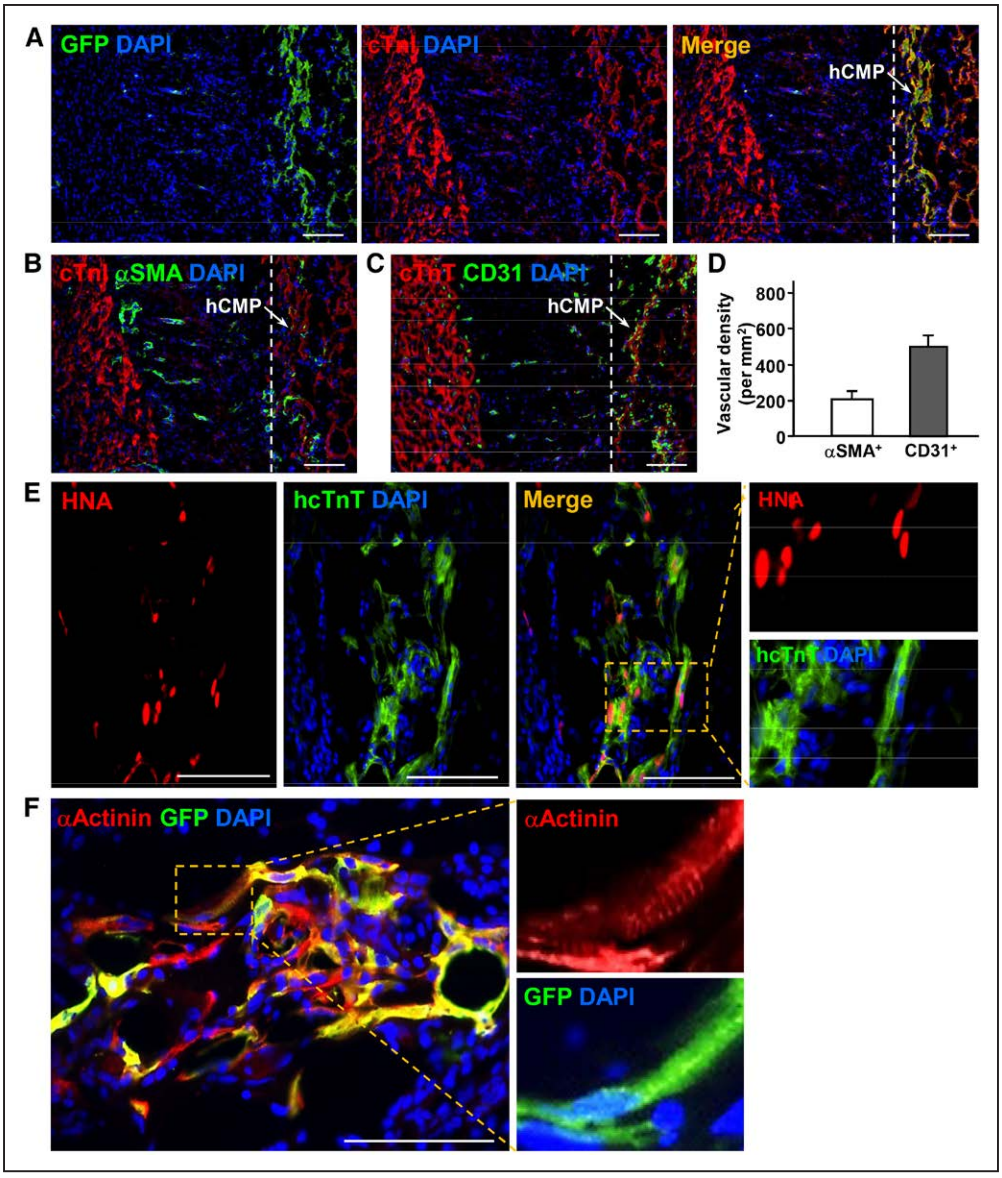

Figure 4. hCMPs engraft and survive after transplantation onto infarcted swine hearts.
Ischemia-reperfusion injury was surgically induced in swine hearts, and then 2 hCMPs were sutured over the site of infarction. Sections taken at week 4 from the region of patch application were immunofluorescently stained for the presence of cTnI, cTnT, GFP, human specific nuclear antigen (HNA), human specific TnT (hcTnT), α-sarcomeric actinin (αActinin), αSMA, human specific calponin 1 (hCalponin 1), CD31, and the human isoform of CD31 (hCD31); nuclei were counterstained with DAPI. **A**, Engrafted hiPSC-CMs were identified by the coexpression of GFP and cTnI; the transplanted hCMP is located to the right of the dashed line in the merged image. **B** through **D**, Vascular structures were identified via the presence of αSMA (**B**) or CD31 expression (**C**); then, vessel density in the hCMP was quantified by calculating the number of αSMA⁺ or CD31⁺ structures per unit area (**D**). **E**, Engrafted hiPSC-CMs were further identified by the coexpression of HNA or hcTnT. **F**, Evidence of maturing sarcomeric structure (insets) was visible in sections stained for the coexpression of GFP and αActinin. **G** and **H**, hiPSC-SMCs were identified as evidence of arterioles within the engrafted patch via the coexpression of αSMA and GFP (**G**), or hCalponin 1 and αSMA (**H**). **I** and **J**, hiPSC-ECs were identified in the vasculature of the engrafted patch via the expression of CD31 and hCD31 (**I**), and in arterioles within the engrafted patch via the expression of hCD31 and αSMA (**J**). These data indicate that the majority of neovascularization vessels are from angiogenesis, with small portion of the total spouting arterials or arterioles that are involved by vascular genesis. Scale bar=100 μm. cTnI indicates cardiac troponin I; cTnT, cardiac troponin T; hiPSC, human induced-pluripotent stem cell; hiPSC-CMs, hiPSC-derived cardiomyocytes; hi-PSC-EC, hiPSC-derived endothelial cell; DAPI, 4′,6-diamidino-2-phenylindole; GFP, green fluorescent protein; hCMP, human cardiac muscle patch; hcTnT, human-specific isoforms of cTnT; and αSMA, α-smooth muscle actin.

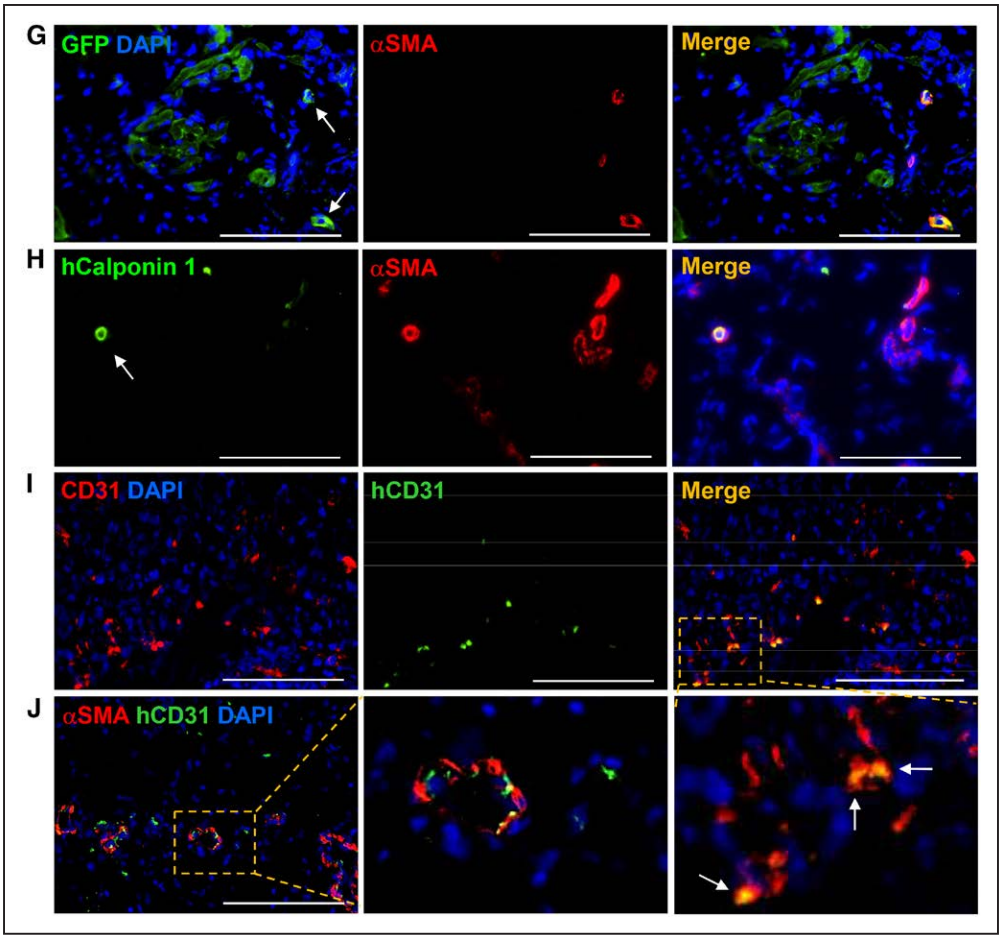

Figure 4 Continued.

MI+hCMP and Sham animals were similar and significantly lower than in MI+OP or MI animals. Thus, the hCMPs appeared to improve cardiac function, reduce wall stress and infarct size, and limit myocardial remodeling when transplanted over the infarcted region of swine hearts.

hCMP Transplantation Does Not Induce Ventricular Arrhythmia

Because the potential for arrythmogenic complications may be the most prominent safety concern associated with CM transplantation,[27] loop recorders were implanted in a subset of animals from the MI, MI+OP, and MI+hCMP groups, and ECGs were continuously monitored from before MI induction until 4 weeks afterward. Although severe arrhythmias and ST-segment elevations occurred in all animals (MI: n=6, MI+OP: n=7, MI+hCMP: n=5) during occlusion and reperfusion and within the first 14 days after the MI, however, after the initial 14 days post-acute MI, no animal in any group developed spontaneous arrhythmia during the remaining 2-week follow-up period. Furthermore, incidents of ventricular tachycardia or ventricular fibrillation were not significantly different between the different groups based on the loop recorder data. In response to programmed electric stimulation protocol, there was no significantly increased arrhythmogenicity among the different groups of hearts. Thus, hCMP transplantation did not adversely affect the electric stability of infarcted swine hearts.

hCMPs Secrete Exosomes That Promote CM Proliferation and Cell-Cycle Progression, Enhance the Angiogenic Activity of ECs, and Protect CMs From Hypoxic Damage

The potentially important role of exosomes in myocardial repair and protection is just beginning to be recognized[28,29]; thus, we studied whether the beneficial paracrine activity associated with hCMP transplantation may have been partially mediated by secreted exosomes. Nanoparticle tracking (Figure 6A) and transmission electron microscopy (Figure 6B) analyses indicated that the exosomes in the hCMP culture medium were typically ≈100 nm in diameter and had bilayered

ORIGINAL RESEARCH ARTICLE

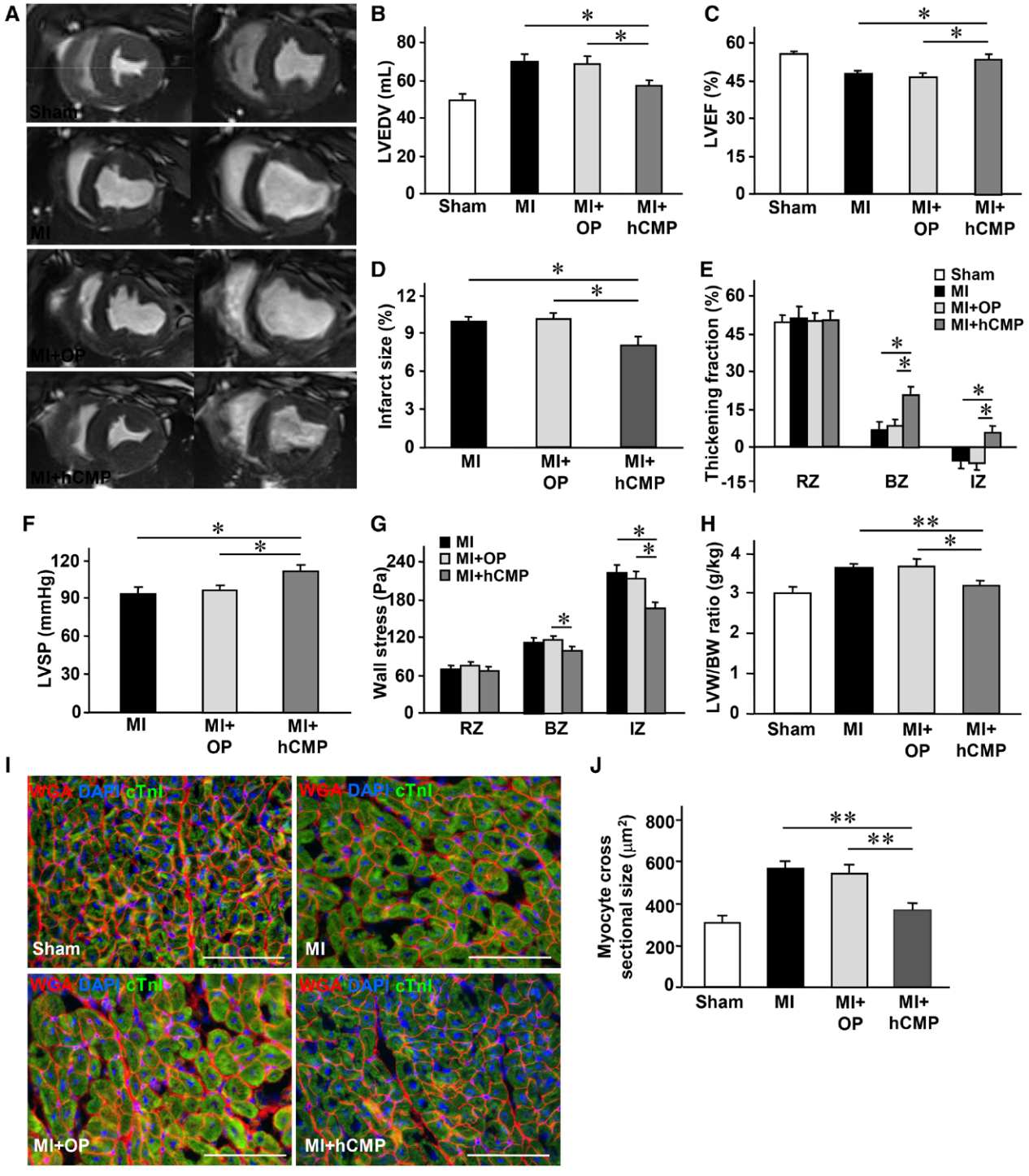

Figure 5. hCMP transplantation improves the recovery of cardiac function and limits adverse remodeling in infarcted pig hearts.

MI was surgically induced in swine hearts by occluding the coronary artery for 60 minutes; then, 2 hCMPs were sutured over the site of infarction in animals from the MI+hCMP group, 2 large fibrin patches lacking the hiPSC-derived cardiac cells were sutured over the injury site in animals from the MI+OP group, and animals in the MI group recovered without either experimental treatment. Animals in the Sham group underwent all surgical procedures for MI induction, with the exception of the occlusion step. **A** through **E**, Four weeks after MI or Sham surgery, magnetic resonance images (**A**) (**Left**, end systole; **Right**, end diastole) were obtained and used to measure left ventricular end-diastolic volumes (LVEDV) (**B**), left ventricular ejection fractions (LVEF) (**C**), infarct sizes (**D**), and systolic thickening fractions (**E**) in the infarcted zone (IZ) of the LV wall, in the border zone (BZ) of the infarct, and in a remote (ie, noninfarcted) zone (RZ). n=8 to 10 per experimental group. **F**, (*Continued*)

membranes, whereas Western blots confirmed the presence of the exosomal marker proteins ALG-2-interacting protein X (Alix), tumor susceptibility gene 101 protein (TSG101), CD81, CD63, and CD9 (Figure 6C). Furthermore, images of PKH26 fluorescence indicated that when CMs were cultured with PKH26-labeled exosomes, the number of exosomes taken up by the cultured cells increased substantially over 24 hours, which were inhibited by pretreatment with the exosome internalization inhibitor, annexin V[30] (Figure 6D).

When cultured with hCMP-secreted exosomes, expression of the proliferation marker Ki67 (Figure VIA in the online-only Data Supplement), the M-phase marker phosphorylated histone 3 (Figure VIB in the online-only Data Supplement), and the cytokinesis marker Aurora B (Figure VIC in the online-only Data Supplement) increased significantly in hiPSC-CMs. hCMP-secreted exosomes also promoted tube formation (Figure VIIA and VIIB in the online-only Data Supplement) and migration (Figure VIIC in the online-only Data Supplement) in cultured hiPSC-ECs. Furthermore, measurements of lactate dehydrogenase leakage (Figure 6E), cell viability (Figure 6F), and apoptosis (Figure 6G and 6H) indicated that hCMP-secreted exosomes protected cultured CMs from the cytotoxic effects associated with serum-free hypoxic media, but not when pretreated with inhibitors of exosome release (GW4869) or internalization (annexin V). Exosomes isolated from cocultures of hiPSC-ECs and -SMCs also protected cultured CMs from serum-free and hypoxic injury, and exosomes obtained from all 3 hiPSC-derived cell types were significantly more protective than those from hiPSC-CMs alone (Figure 6I and 6J). Collectively, these observations suggest that hCMP-secreted exosomes may contribute to the beneficial effects associated with hCMP transplantation by promoting CM proliferation and cell-cycle activity, enhancing the neovascularization activity of ECs, and protecting ischemic infarct boarder zone myocytes from apoptosis.

hCMP Transplantation Promotes Angiogenesis and Cell Survival in the Periscar BZ After MI

It is known that CMs function better when there are ECs within the microenvironment. However, it remains too low (11% of 16 million cells delivered) to account for the observed improvements in LV chamber function and infarct size reduction, unless the cells promoted the activity of beneficial paracrine mechanisms. Therefore, we investigated whether hCMP transplantation may have improved the recovery of infarcted hearts by promoting the activity of mechanisms that contribute to myocardial repair and protection. The number of vascular structures either expressing CD31 (Figure 7A and 7B) or coexpressing CD31 and αSMA (Figure 7A and 7C), and the number of cells expressing the proliferation marker Ki67 (Figure 7D and 7E), as well, was significantly higher in the BZ of hearts from MI+hCMP animals than in the corresponding regions of hearts from MI+OP or MI animals. The BZ of hearts from hCMP-treated animals also had significantly fewer apoptotic (ie, terminal deoxynucleotidyltransferase dUTP nick end labeling–positive) cells (Figure 7F and 7G) and significantly higher levels of the prosurvival proteins erythropoietin, hepatocyte growth factor, and angiopoietin 1 (Ang1) (Figure 7H and 7I). Collectively, these results suggest that the benefits of hCMP transplantation likely occurred, at least in part, through paracrine mechanisms that promote the growth of blood vessels and arterioles, and cell proliferation and survival, as well.

hCMP Transplantation Partially Prevents or Reverses MI-Induced Changes in Sarcomeric Protein Phosphorylation

Studies have demonstrated that the phosphorylation states of sarcomeric proteins are altered by MI, and that these alterations correlate with contractile dysfunction[31,32]; thus, we conducted top-down proteomics analysis[33] (Figure VIII in the online-only Data Supplement) to determine whether the improvements in cardiac function observed in MI+hCMP animals were accompanied by the normalization of sarcomeric protein phosphorylation. cTnT (Figure 8A) and myosin light chain 2 (Figure 8B) phosphorylation levels did not change significantly in response to MI injury or subsequent hCMP transplantation, and although α-tropomyosin (αTpm) (Figure 8C) and βTpm (Figure 8D) phosphorylation was significantly higher in MI than in Sham animals, measurements were similarly elevated in animals from the MI+hCMP group. However, measurements of cTnI (Figure 8E) and enigma homolog isoform 2 (Figure 8F) phosphorylation in the MI+hCMP

Figure 5 Continued. Hemodynamic measurements. **G**, End-systolic LV wall stress in the IZ, BZ, and RZ. n=5 to 7 per experimental group. **H** through **J,** Animals were euthanized at week 4; then, the LV weight to body weight (LVW/BW) ratios were determined (n=8–11 per experimental group) (**H**). **I** and **J**, Sections from the border zone of the infarct were collected and stained with wheat germ agglutinin (WGA) and cTnI to visualize cardiomyocytes (n=6–8 per experimental group, scale bar=100 μm) (**I**). Nuclei were counterstained with DAPI, and cardiomyocyte cross-sectional surface areas were measured (**J**). **P*<0.05. ***P*<0.01. cTnI indicates cardiac troponin I; DAPI, 4′,6-diamidino-2-phenylindole; hCMP, human cardiac muscle patch; hiPSC, human induced-pluripotent stem cell; LV, left ventricle; MI, myocardial infarction; and OP, open fibrin patches.

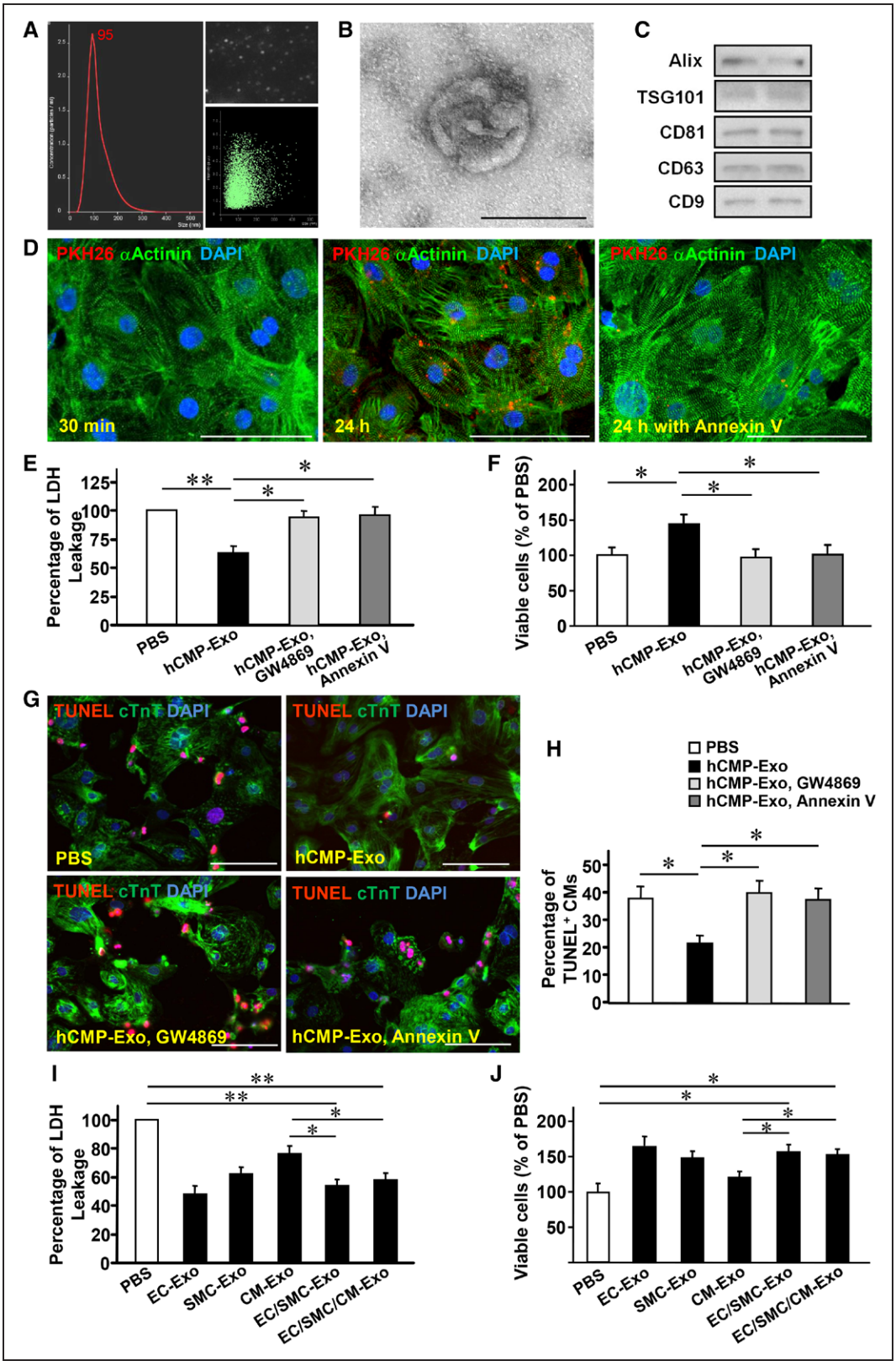

Figure 6. Characteristics and cytoprotective effects of hCMP-secreted exosomes.
Exosomes were isolated from the hCMP culture medium; then, exosome size was evaluated via nanoparticle tracking analysis (**A**), exosome morphology was evaluated via electron microscopy (bar=100 nm) (**B**), and the presence of exosome marker proteins (ALG-2-interacting protein X [Alix], tumor susceptibility gene 101 protein [TSG101], CD81, CD63, CD9) was evaluated via Western blot (**C**). **D**, Cardiomyocytes were incubated for 30 minutes or 24 hours with PKH26-labeled (*Continued*)

and Sham groups were similar and significantly greater than in MI animals. Taken together, these results indicate that hCMP transplantation may prevent or reverse at least some of the changes in the phosphorylation of these key sarcomeric regulatory proteins that occur in response to MI; this previously unrecognized mechanism may be partially responsible for the improved myocardial contractility observed in hCMP-treated animals.

DISCUSSION

The present study is the first to evaluate hCMPs with trilineage cardiac cells and with clinically relevant dimensions (4 cm × 2 cm × 1.25 mm) in a large-animal model of ischemic myocardial injury. The hCMPs were cultured under dynamic (rocking) conditions for 1 week, which results in a prominent force generation of 1.1 nN/myocyte (Figure 3N) of the fabricated hCMP. After 7 days of dynamic culture, a superior physiological function of the novel fabricated hCMP was achieved, which is evidenced by the functional assessments of conductive velocity, calcium transients, microimpedence, and twitch-force generation. These functional data demonstrate that the mechanisms related to the intercellular communication, calcium handling, and force generation were significantly improved during the 7-day dynamic culture stimulation. The engraftment rate for the transplanted cells exceeded 10% at week 4. The exosome released from the hCMP results in significant reduction of myocyte apoptosis in vitro. The treatment of novel hCMP with CMs, ECs, and SMCs was associated with significant improvements in LV wall stress, infarct size, vascular density, apoptosis, and prevented/reversed maladaptive changes in the phosphorylation states of sarcomeric proteins in BZ myocardium. The hCMP did not increase the risk of arrhythmogenic complications.

It is well known that cardiac myocytes survive and function much better in the microenvironment with the copresence of ECs than the microenvironment with myocytes only. In the present study, the hCMP superior functional level based on the mechanical and electrophysiological performance is likely contributed, in part, by the trilineage cardiac cell presence within the engineered tissue (Figure 2). The graft of hiPSC-derived cardiac cells can contribute directly to cardiac function, but they are also less mature than the native cardiac cells of adult hearts, which could lead to safety concerns. The gene-expression profile, and a variety of structural and functional properties, as well, of hiPSC-CMs more closely resembles that of neonatal CMs than of adult CMs.[6,34] The abnormal calcium transients or electrophysiological properties in engrafted CMs may cause regional variations in repolarization.[28] These observations may partially explain why hPSC-CMs, and even allogeneic monkey iPSC-derived CMs, led to incidents of spontaneous arrhythmia when studied in a nonhuman primate MI model.[2,5] Therefore, the electrophysiologically more mature hCMPs (Figure 3A through 3K) with the trilineage cardiac cells under this dynamic culture condition may have better translational potential.

The CMs present in 3-dimensional, engineered heart tissue appear to be more mature than those obtained via monolayer culturing techniques.[6,11,16] For the experiments presented here, maturation was further promoted by rocking the hCMPs during culture and by using trilineage cardiac cells that had been differentiated from cardiac-lineage hciPSCs[16] (rather than hiPSCs of dermal or other lineages). Our analyses confirmed that the expression of genes involved in contraction and calcium-transient generation was significantly greater in the hCMPs than in monolayer-cultured CMs (Figure II in the online-only Data Supplement), and in hCMPs that were cultured under dynamic rather than static conditions.[9] Furthermore, the conduction veloc-

Figure 6 Continued. hCMP-secreted exosomes that had been pretreated with or without the exosome uptake inhibitor annexin V (2 μg/mL); then, the cardiomyocytes were fixed and immunofluorescently stained for α-actinin, nuclei were counterstained with DAPI, and exosomes that had been taken up by the cardiomyocytes were identified by PKH26 fluorescence (bar=100 μm). **E** through **H**, Cardiomyocytes were cultured under hypoxic conditions in serum-free Dulbecco modified Eagle medium (DMEM) for 48 hours with phosphate-buffered saline (PBS) or with exosomes from hCMPs (hCMP-Exo) that had been treated with or without an exosome-release inhibitor (GW4869, 10 μmol/L) or an exosome-internalization inhibitor (annexin V, 2 μg/mL). **E**, The intensity of lactate dehydrogenase (LDH) fluorescence observed in the media was measured and expressed as a percentage of the intensity observed in PBS-cultured cells. **F**, Cell viability was measured with a colorimetric assay that detected the reduction of a tetrazolium compound into a colored formazan product (the conversion occurs through the metabolic activity of living cells), and expressed as a percentage of the measurement in PBS group. **G**, Cardiomyocytes were fixed, immunofluorescently stained for cTnT expression and TUNEL stained; nuclei were counterstained with DAPI (bar=100 μm). **H**, Apoptosis was quantified as the percentage of cells that were TUNEL positive. **I** and **J**, Cardiomyocytes were cultured under hypoxic conditions for 48 hours in serum-free DMEM medium and treated with PBS or with exosomes collected from monolayer cultures of ECs (EC-Exo), SMCs (SMC-Exo), or cardiomyocytes (CM-Exo), from a coculture of ECs and SMCs (EC/SMC-Exo), or from a coculture of all 3 cell types (EC/SMC/CM-Exo). Cytotoxicity was evaluated via measurements of cardiomyocytes LDH leakage (**I**) and cell viability(**J**). *P<0.05, **P<0.01. n=4 to 5 experiments. CM indicates cardiomyocyte; cTnT, cardiac troponin T; DAPI, 4′,6-diamidino-2-phenylindole; EC, endothelial cell; hCMP, human cardiac muscle patch; SMC, smooth muscle cell; and TUNEL, terminal deoxynucleotidyl transferase dUTP nick end labeling.

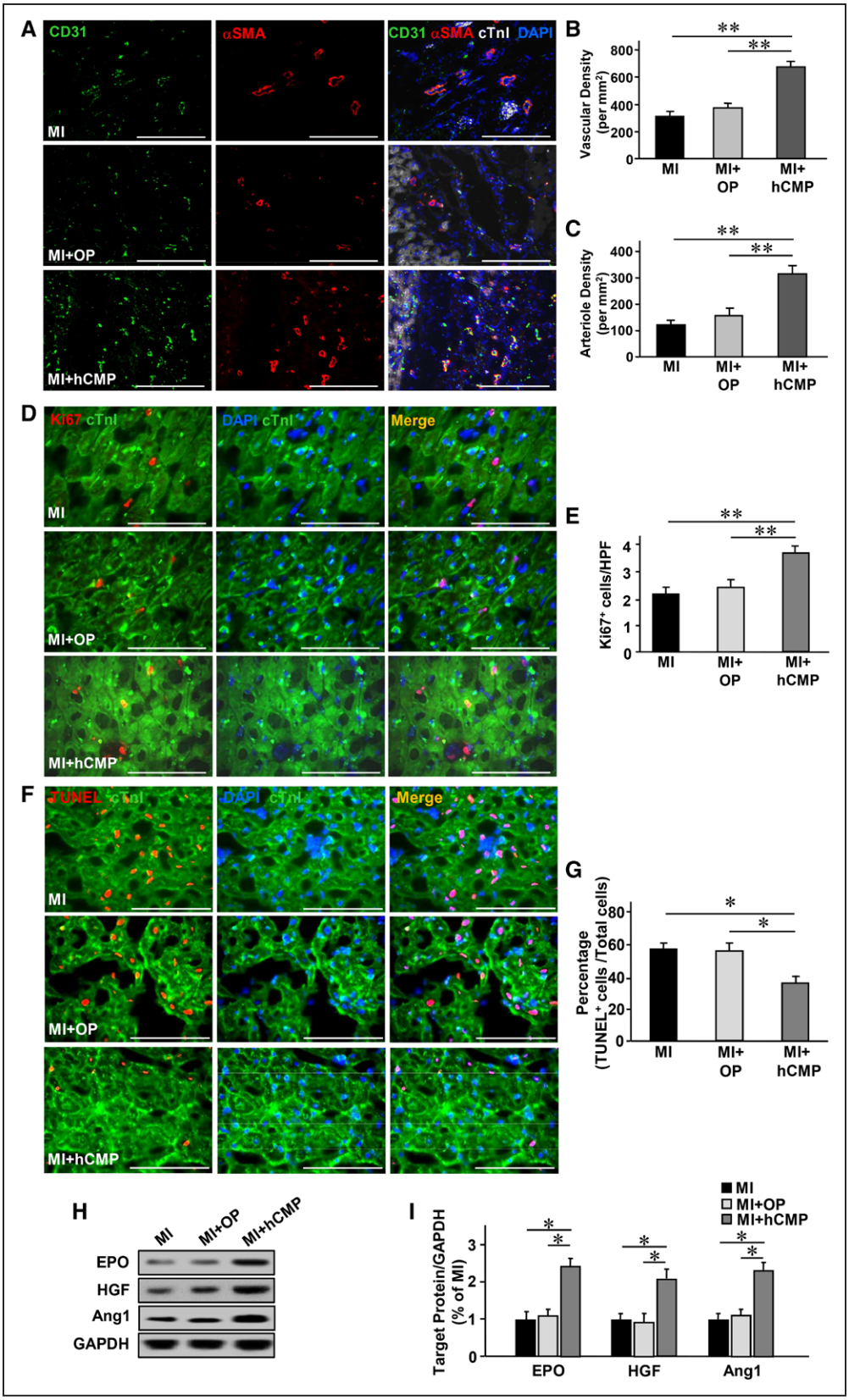

Figure 7. hCMP transplantation enhances the vasculogenic response, promotes cell proliferation, and reduces apoptosis after MI.

Sections were collected from the border-zone of the infarct in MI, MI+OP, and MI+hCMP animals 4 weeks after MI induction. **A**, Sections were stained with fluorescent antibodies against CD31, αSMA, and cTnI (bar=200 μm), and nuclei (*Continued*)

ity in our hCMPs reached 14.1±1.0 cm/s, which is consistent with observations from other laboratories,[35] and suggests that mechanisms for gap-junction connectivity and action-potential initiation[36,37] functioned with efficiency within the structure of the novel hCMP. The enhanced electromechanical coupling of CMs in the hCMPs was also evident from analyses of resistivity-reactivity spectra (Figure 3E and 3F), which suggested that intercellular gap-junction communication in the hCMPs and in native rabbit LV myocardium[38] was similar. Similarly, the superior functional performance of the hCMP was evidenced by the assessments of contractile force per CM, calcium-transient dynamics, responsiveness to a β-adrenergic agonist, the Frank-Starling mechanism,[10] and the dependence of twitch force on pacing frequency and calcium concentration (Figure 3).

The porosity of the hCMP (Figure 2) likely improved the diffusion of nutrients and oxygen, which is particularly important for patches of this size, and could have improved engraftment by facilitating in-growth of angiogenesis (Figure 4B through 4D). The unique spatial relationship of the ECs and CMs (Figure 2F and Figure IIIC in the online-only Data Supplement) may have contributed to the superior functional characteristics the novel hCMPs of this size.

The electrophysiological activity of the hCMPs is also likely to have been influenced by the inclusion of hiPSC-SMCs and -ECs in the hCMP. Endothelial cells have been shown to improve recovery from myocardial injury, regulate cardiovascular physiology, and promote the survival of transplanted CMs primarily by activating cytokine-associated mechanisms. The results from experiments in our laboratory indicate that CMs are more resistant to hypoxia-induced apoptosis and lactate dehydrogenase leakage when cultured with EC- and SMC-conditioned medium.[3] Furthermore, the data presented here suggest that at least some of the cytoprotective effects associated with ECs and SMCs are mediated by exosome release (Figure 6), and the exosomes may also carry paracrine factors that contributed to the observed increases in angiogenesis and native CM proliferation. Collectively, these paracrine mechanisms, and the microenvironment of the patch itself, likely contributed to the relatively high engraftment rate (10.9±1.8%), which is consistent with the results from studies in rodents.[4,11,15]

Our top-down proteomics analyses confirmed that 4 weeks after MI injury, phosphorylation of the sarcomeric proteins enigma homolog isoform 2 and cTnI was significantly reduced in animals from the MI group, which is consistent with the results from previous studies,[31,32] and that these reductions were prevented (or reversed) in MI+hCMP animals. The hCMP-associated increase in cTnI phosphorylation may be particularly relevant, because reports from other groups indicate that declines in cTnI phosphorylation can contribute to contractile dysfunction after MI or during end-stage heart failure by increasing myofilament Ca^{2+} sensitivity.[32,39] Thus, these results are the first to suggest that hiPSC-derived cardiac cells may improve contractile function in infarcted hearts by preventing or reversing maladaptive changes in the phosphorylation states of sarcomeric proteins.

The experiments presented in this report are the first to evaluate a novel type of hCMP of clinically relevant dimensions (4 cm × 2 cm × 1.25 mm) in a large-animal model of ischemic myocardial injury. In vitro assessments indicated that the machinery required for calcium handling and force generation of CMs within the hCMP was relatively well developed in response to the dynamic culture stimulation for 7 days. When tested in a porcine MI model, the engraftment rate for the transplanted cells exceeded 10% at week 4, and the treatment was associated with improvements in LV dilatation, wall stress, infarct size, and preventing/reversing maladaptive changes in the phosphorylation states of sarcomeric proteins in BZ myocardium. The hCMP therapy did not increase the risk of arrhythmia.

Figure 7 Continued. were counterstained with DAPI; then, vascular density was determined by quantifying the number of structures that expressed CD31 (**B**), and arteriole density was determined by quantifying the number of structures that expressed both CD31 and αSMA (**C**). **D**, Sections were stained for expression of the cell proliferation marker Ki67, muscle fibers were visualized by fluorescent immunostaining for cTnI, and nuclei were counterstained with DAPI (bar=100 μm); then, cell proliferation was quantified as the number of Ki67-positive cells per high-power field (HPF) (n=6–8 per experimental group) (**E**). **F**, Sections taken from the border zone of infarction at week 1 after MI were stained with antibodies against cTnI, apoptotic cells were identified via a TUNEL staining, and nuclei were counterstained with DAPI (bar=100 μm); then, apoptosis was quantified as the percentage of cells that were positive for TUNEL staining (n=3–4 in each group) (**G**). **H**, Expression of the prosurvival proteins erythropoietin (EPO), hepatocyte growth factor (HGF), and angiopoietin 1 (Ang1) at week 1 after MI were evaluated in tissues from the border zone of infarction via Western blot. Glyceraldehyde phosphate dehydrogenase (GAPDH) protein levels were evaluated to serve as a control for unequal loading. **I**, EPO, HGF, and Ang1 protein levels were quantified via densitometry analysis and normalized to GAPDH protein levels (n=3 in each group). **P*<0.05, ***P*<0.01. cTnI indicates cardiac troponin I; DAPI, 4′,6-diamidino-2-phenylindole; hCMP, human cardiac muscle patch; MI, myocardial infarction; OP, open fibrin patches; αSMA, α-smooth muscle actin; and TUNEL, terminal deoxynucleotidyl transferase dUTP nick end labeling.

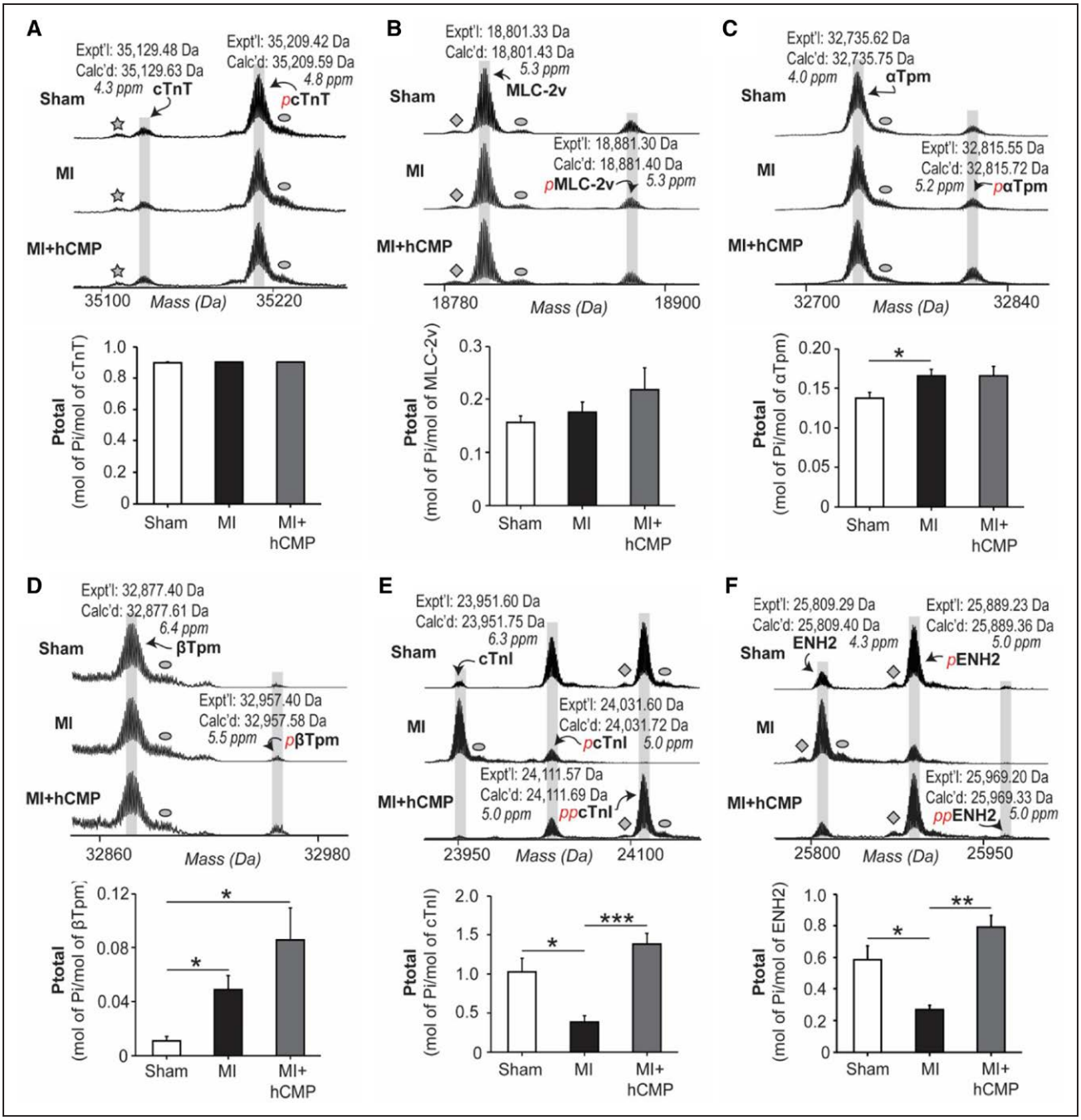

Figure 8. MI-induced changes in sarcomeric protein phosphorylation are partially prevented or reversed by hCMP transplantation.

Four weeks after MI induction, phosphorylation of the sarcomeric proteins, cTnT (**A**), MLC-2v (**B**), α-tropomyosin (αTpm) (**C**), βTpm (**D**), cTnI (**E**), and enigma homolog isoform 2 (ENH2) (**F**), was quantified in myocardium from the border zone of infarction in animals from the MI and MI+hCMP groups and from the corresponding region of hearts in Sham animals via top-down proteomics and mass spectroscopy. The star in the cTnT/pcTnT spectrum identifies a peak caused by the loss of H_3PO_4, diamonds identify peaks caused by the loss of NH_3, and ovals identify peaks caused by oxidation of the protein. **P*<0.05, ***P*<0.01, ****P*<0.001. n=6 per experimental group. Calc'd indicates calculated most abundant molecular mass based on the DNA-predicted protein sequence; cTnI, cardiac troponin I; Expt'l, experimentally determined most abundant molecular mass; hCMP, human cardiac muscle patch; MI, myocardial infarction; and MLC-2v, myosin light chain 2v.

ARTICLE INFORMATION

Received July 28, 2017; accepted November 20, 2017.

The online-only Data Supplement is available with this article at http://circ.ahajournals.org/lookup/suppl/doi:10.1161/CIRCULATIONAHA.117.030785/-/DC1.

Correspondence

Jianyi (Jay) Zhang, MD, PhD, Department of Biomedical Engineering, School of Medicine and School of Engineering, University of Alabama at Birmingham, 1670 University Blvd, Volker Hall G094J, Birmingham, AL 35233. E-mail jayzhang@uab.edu

Affiliations

Department of Biomedical Engineering, School of Medicine and School of Engineering, University of Alabama at Birmingham (L.G., W.Z., S.M., Y.O., X.LO., R.K., A.V.B., G.P.W., A.E.P., V.G.F., S.G.L., J.Z.). Department of Cell and Regenerative Biology, University of Wisconsin-Madison (Z.R.G., Y.G.). Second Affiliated Hospital, College of Medicine, Zhejiang University, Hangzhou, China (X.H.).

Acknowledgments

The authors thank Dr W. Kevin Cukier-Meisner for editorial assistance with the completion of this article, and Dr Yanwen Liu for excellent technical assistance.

Sources of Funding

This work was supported by the following funding sources: NIH RO1 HL 99507, HL114120, HL 131017, UO1 HL134764 (to Dr Zhang), NIH F31 HL128086 (to Dr Gregorich), and Shared Instrumentation Grant Program OD018475, NIH R01 HL 109810 (to Dr Ge).

Disclosures

None.

REFERENCES

1. Sayed N, Liu C, Wu JC. Translation of human-induced pluripotent stem cells: from clinical trial in a dish to precision medicine. *J Am Coll Cardiol*. 2016;67:2161–2176. doi: 10.1016/j.jacc.2016.01.083.
2. Shiba Y, Gomibuchi T, Seto T, Wada Y, Ichimura H, Tanaka Y, Ogasawara T, Okada K, Shiba N, Sakamoto K, Ido D, Shiina T, Ohkura M, Nakai J, Uno N, Kazuki Y, Oshimura M, Minami I, Ikeda U. Allogeneic transplantation of iPS cell-derived cardiomyocytes regenerates primate hearts. *Nature*. 2016;538:388–391. doi: 10.1038/nature19815.
3. Ye L, Chang YH, Xiong Q, Zhang P, Zhang L, Somasundaram P, Lepley M, Swingen C, Su L, Wendel JS, Guo J, Jang A, Rosenbush D, Greder L, Dutton JR, Zhang J, Kamp TJ, Kaufman DS, Ge Y, Zhang J. Cardiac repair in a porcine model of acute myocardial infarction with human induced pluripotent stem cell-derived cardiovascular cells. *Cell Stem Cell*. 2014;15:750–761. doi: 10.1016/j.stem.2014.11.009.
4. Riegler J, Tiburcy M, Ebert A, Tzatzalos E, Raaz U, Abilez OJ, Shen Q, Kooreman NG, Neofytou E, Chen VC, Wang M, Meyer T, Tsao PS, Connolly AJ, Couture LA, Gold JD, Zimmermann WH, Wu JC. Human engineered heart muscles engraft and survive long term in a rodent myocardial infarction model. *Circ Res*. 2015;117:720–730. doi: 10.1161/CIRCRESAHA.115.306985.
5. Chong JJ, Yang X, Don CW, Minami E, Liu YW, Weyers JJ, Mahoney WM, Van Biber B, Cook SM, Palpant NJ, Gantz JA, Fugate JA, Muskheli V, Gough GM, Vogel KW, Astley CA, Hotchkiss CE, Baldessari A, Pabon L, Reinecke H, Gill EA, Nelson V, Kiem HP, Laflamme MA, Murry CE. Human embryonic-stem-cell-derived cardiomyocytes regenerate non-human primate hearts. *Nature*. 2014;510:273–277. doi: 10.1038/nature13233.
6. Sun X, Nunes SS. Bioengineering approaches to mature human pluripotent stem cell-derived cardiomyocytes. *Front Cell Dev Biol*. 2017;5:19. doi: 10.3389/fcell.2017.00019.
7. Robertson C, Tran DD, George SC. Concise review: maturation phases of human pluripotent stem cell-derived cardiomyocytes. *Stem Cells*. 2013;31:829–837. doi: 10.1002/stem.1331.
8. Tiburcy M, Hudson JE, Balfanz P, Schlick S, Meyer T, Chang Liao ML, Levent E, Raad F, Zeidler S, Wingender E, Riegler J, Wang M, Gold JD, Kehat I, Wettwer E, Ravens U, Dierickx P, van Laake LW, Goumans MJ, Khadjeh S, Toischer K, Hasenfuss G, Couture LA, Unger A, Linke WA, Araki T, Neel B, Keller G, Gepstein L, Wu JC, Zimmermann WH. Defined engineered human myocardium with advanced maturation for applications in heart failure modeling and repair. *Circulation*. 2017;135:1832–1847. doi: 10.1161/CIRCULATIONAHA.116.024145.
9. Jackman CP, Carlson AL, Bursac N. Dynamic culture yields engineered myocardium with near-adult functional output. *Biomaterials*. 2016;111:66–79. doi: 10.1016/j.biomaterials.2016.09.024.
10. Ruan JL, Tulloch NL, Razumova MV, Saiget M, Muskheli V, Pabon L, Reinecke H, Regnier M, Murry CE. Mechanical stress conditioning and electrical stimulation promote contractility and force maturation of induced pluripotent stem cell-derived human cardiac tissue. *Circulation*. 2016;134:1557–1567. doi: 10.1161/CIRCULATIONAHA.114.014998.
11. Gao L, Kupfer ME, Jung JP, Yang L, Zhang P, Da Sie Y, Tran Q, Ajeti V, Freeman BT, Fast VG, Campagnola PJ, Ogle BM, Zhang J. Myocardial tissue engineering with cells derived from human-induced pluripotent stem cells and a native-like, high-resolution, 3-dimensionally printed scaffold. *Circ Res*. 2017;120:1318–1325. doi: 10.1161/CIRCRESAHA.116.310277.
12. Ogle BM, Bursac N, Domian I, Huang NF, Menasché P, Murry CE, Pruitt B, Radisic M, Wu JC, Wu SM, Zhang J, Zimmermann WH, Vunjak-Novakovic G. Distilling complexity to advance cardiac tissue engineering. *Sci Transl Med*. 2016;8:342ps13. doi: 10.1126/scitranslmed.aad2304.
13. Nguyen PK, Neofytou E, Rhee JW, Wu JC. Potential strategies to address the major clinical barriers facing stem cell regenerative therapy for cardiovascular disease: a review. *JAMA Cardiol*. 2016;1:953–962. doi: 10.1001/jamacardio.2016.2750.
14. Tzatzalos E, Abilez OJ, Shukla P, Wu JC. Engineered heart tissues and induced pluripotent stem cells: macro- and microstructures for disease modeling, drug screening, and translational studies. *Adv Drug Deliv Rev*. 2016;96:234–244. doi: 10.1016/j.addr.2015.09.010.
15. Weinberger F, Breckwoldt K, Pecha S, Kelly A, Geertz B, Starbatty J, Yorgan T, Cheng KH, Lessmann K, Stolen T, Scherrer-Crosbie M, Smith G, Reichenspurner H, Hansen A, Eschenhagen T. Cardiac repair in guinea pigs with human engineered heart tissue from induced pluripotent stem cells. *Sci Transl Med*. 2016;8:363ra148. doi: 10.1126/scitranslmed.aaf8781.
16. Zhang D, Shadrin IY, Lam J, Xian HQ, Snodgrass HR, Bursac N. Tissue-engineered cardiac patch for advanced functional maturation of human ESC-derived cardiomyocytes. *Biomaterials*. 2013;34:5813–20. doi: 10.1016/j.biomaterials.2013.04.026.
17. Zhang L, Guo J, Zhang P, Xiong Q, Wu SC, Xia L, Roy SS, Tolar J, O'Connell TD, Kyba M, Liao K, Zhang J. Derivation and high engraftment of patient-specific cardiomyocyte sheet using induced pluripotent stem cells generated from adult cardiac fibroblast. *Circ Heart Fail*. 2015;8:156–66. doi: 10.1161/CIRCHEARTFAILURE.114.001317.
18. Lux M, Andrée B, Horvath T, Nosko A, Manikowski D, Hilfiker-Kleiner D, Haverich A, Hilfiker A. *In vitro* maturation of large-scale cardiac patches based on a perfusable starter matrix by cyclic mechanical stimulation. *Acta Biomater*. 2016;30:177–187. doi: 10.1016/j.actbio.2015.11.006.
19. Ye L, Zimmermann WH, Garry DJ, Zhang J. Patching the heart: cardiac repair from within and outside. *Circ Res*. 2013;113:922–932. doi: 10.1161/CIRCRESAHA.113.300216.
20. Xiong Q, Ye L, Zhang P, Lepley M, Swingen C, Zhang L, Kaufman DS, Zhang J. Bioenergetic and functional consequences of cellular therapy: activation of endogenous cardiovascular progenitor cells. *Circ Res*. 2012;111:455–468. doi: 10.1161/CIRCRESAHA.112.269894.
21. Burridge PW, Matsa E, Shukla P, Lin ZC, Churko JM, Ebert AD, Lan F, Diecke S, Huber B, Mordwinkin NM, Plews JR, Abilez OJ, Cui B, Gold JD, Wu JC. Chemically defined generation of human cardiomyocytes. *Nat Methods*. 2014;11:855–860. doi: 10.1038/nmeth.2999.
22. Lian X, Zhang J, Azarin SM, Zhu K, Hazeltine LB, Bao X, Hsiao C, Kamp TJ, Palecek SP. Directed cardiomyocyte differentiation from human pluripotent stem cells by modulating Wnt/β-catenin signaling under fully defined conditions. *Nat Protoc*. 2013;8:162–175. doi: 10.1038/nprot.2012.150.
23. Zhang S, Dutton JR, Su L, Zhang J, Ye L. The influence of a spatiotemporal 3D environment on endothelial cell differentiation of human induced pluripotent stem cells. *Biomaterials*. 2014;35:3786–3793. doi: 10.1016/j.biomaterials.2014.01.037.
24. Sequeira V, van der Velden J. Historical perspective on heart function: the Frank-Starling Law. *Biophys Rev*. 2015;7:421–447. doi: 10.1007/s12551-015-0184-4.

25. Wendel JS, Ye L, Tao R, Zhang J, Zhang J, Kamp TJ, Tranquillo RT. Functional effects of a tissue-engineered cardiac patch from human induced pluripotent stem cell-derived cardiomyocytes in a rat infarct model. *Stem Cells Transl Med*. 2015;4:1324–1332. doi: 10.5966/sctm.2015-0044.
26. Wang X, Huang W, Liu G, Cai W, Millard RW, Wang Y, Chang J, Peng T, Fan GC. Cardiomyocytes mediate anti-angiogenesis in type 2 diabetic rats through the exosomal transfer of miR-320 into endothelial cells. *J Mol Cell Cardiol*. 2014;74:139–150. doi: 10.1016/j.yjmcc.2014.05.001.
27. Anderson ME, Goldhaber J, Houser SR, Puceat M, Sussman MA. Embryonic stem cell-derived cardiac myocytes are not ready for human trials. *Circ Res*. 2014;115:335–338. doi: 10.1161/CIRCRESAHA.114.304616.
28. Jung JH, Fu X, Yang PC. Exosomes generated from iPSC-derivatives: new direction for stem cell therapy in human heart diseases. *Circ Res*. 2017;120:407–417. doi: 10.1161/CIRCRESAHA.116.309307.
29. Waldenström A, Ronquist G. Role of exosomes in myocardial remodeling. *Circ Res*. 2014;114:315–324. doi: 10.1161/CIRCRESAHA.114.300584.
30. Li J, Liu K, Liu Y, Xu Y, Zhang F, Yang H, Liu J, Pan T, Chen J, Wu M, Zhou X, Yuan Z. Exosomes mediate the cell-to-cell transmission of IFN-α-induced antiviral activity. *Nat Immunol*. 2013;14:793–803. doi: 10.1038/ni.2647.
31. Peng Y, Gregorich ZR, Valeja SG, Zhang H, Cai W, Chen YC, Guner H, Chen AJ, Schwahn DJ, Hacker TA, Liu X, Ge Y. Top-down proteomics reveals concerted reductions in myofilament and Z-disc protein phosphorylation after acute myocardial infarction. *Mol Cell Proteomics*. 2014;13:2752–2764. doi: 10.1074/mcp.M114.040675.
32. van der Velden J, Merkus D, Klarenbeek BR, James AT, Boontje NM, Dekkers DH, Stienen GJ, Lamers JM, Duncker DJ. Alterations in myofilament function contribute to left ventricular dysfunction in pigs early after myocardial infarction. *Circ Res*. 2004;95:e85–e95. doi: 10.1161/01.RES.0000149531.02904.09.
33. Cai W, Tucholski TM, Gregorich ZR, Ge Y. Top-down proteomics: technology advancements and applications to heart diseases. *Expert Rev Proteomics*. 2016;13:717–730. doi: 10.1080/14789450.2016.1209414.
34. Yang X, Pabon L, Murry CE. Engineering adolescence: maturation of human pluripotent stem cell-derived cardiomyocytes. *Circ Res*. 2014;114:511–523. doi: 10.1161/CIRCRESAHA.114.300558.
35. Jackman CP, Shadrin IY, Carlson AL, Bursac N. Human cardiac tissue engineering: from pluripotent stem cells to heart repair. *Curr Opin Chem Eng*. 2015;7:57–64. doi: 10.1016/j.coche.2014.11.004.
36. Herron TJ, Lee P, Jalife J. Optical imaging of voltage and calcium in cardiac cells & tissues. *Circ Res*. 2012;110:609–623. doi: 10.1161/CIRCRESAHA.111.247494.
37. Kong W, Fakhari N, Sharifov OF, Ideker RE, Smith WM, Fast VG. Optical measurements of intramural action potentials in isolated porcine hearts using optrodes. *Heart Rhythm*. 2007;4:1430–1436. doi: 10.1016/j.hrthm.2007.07.002.
38. Waits CM, Barr RC, Pollard AE. Sensor spacing affects the tissue impedance spectra of rabbit ventricular epicardium. *Am J Physiol Heart Circ Physiol*. 2014;306:H1660–H1668. doi: 10.1152/ajpheart.00661.2013.
39. Messer AE, Jacques AM, Marston SB. Troponin phosphorylation and regulatory function in human heart muscle: dephosphorylation of Ser23/24 on troponin I could account for the contractile defect in end-stage heart failure. *J Mol Cell Cardiol*. 2007;42:247–259. doi: 10.1016/j.yjmcc.2006.08.017.